

Two-step charge photogeneration dynamics in polymer/fullerene blends for photovoltaic applications

Sanjeev Singh,^{1,*†} Bill Pandit,^{1,†} Tek P. Basel,¹ Sergey Li,² Darin Laird,² and Z. Valy Vardeny^{1,‡}

¹*Department of Physics and Astronomy, University of Utah, Salt Lake City, Utah 84112, USA*

²*Plextronics, 2180 William Pitt Way, Pittsburgh, PA 15238*

(Received 5 January 2012; revised manuscript received 16 April 2012; published 15 May 2012)

We measured the picoseconds (ps) transient dynamics of photoexcitations in blends of poly(3-hexyl-thiophene) (P3HT; donors-D) and fullerene [6,6]-phenyl-C₆₁-butyric acid methyl ester (PCBM; acceptor-A), using the transient pump/probe photomodulation technique in an unprecedented broad spectral range from 0.25 to 2.5 eV, and compared the results with organic solar cell performance based on the same blends. In D-A blends with maximum domain separation such as regio-regular P3HT/PCBM with (1.2:1) weight ratio having solar cell power conversion efficiency of $\sim 4\%$, we found that, although the photogenerated intrachain excitons in the polymer nano-domains decay within ~ 10 ps, no charge polarons are generated on their expense up to ~ 2 ns. Instead, there is a buildup of charge transfer (CT) excitons at the D-A interfaces having the same kinetics as the exciton decay, which dissociate into separate polarons in the D and A domains at a much later time ($\gg 1$ ns). This two-step charge photogeneration process may be typical in organic bulk heterojunction cells. Although the CT excitons are photogenerated on the exciton expense much faster in D-A blends having smaller domain size such as in regio-random P3HT/PCBM, their dissociation is less efficient because of larger binding energy. This explains the poor solar cell power conversion efficiency ($< 0.1\%$) based on this blend. Our results support the two-step charge photogeneration mechanism in polymer/fullerene blends and emphasize the important role of the CT binding energy in generating free charge polarons in organic solar cells.

DOI: [10.1103/PhysRevB.85.205206](https://doi.org/10.1103/PhysRevB.85.205206)

PACS number(s): 78.66.Qn, 78.40.Me, 78.45.+h, 78.47.-p

The process of charge photogeneration in organic photovoltaic (OPV) cells is still a matter of debate. In contrast to the labyrinth photosynthesis process that has evolved in nature,¹ the charge photogeneration process in OPV cells utilizes one type of heterojunction between two organic semiconductors. The two organic semiconductors, dubbed donor (D-) and acceptor (A-) are cast from solution mixtures to form thin films having nanosize domains of relatively pristine materials and large D-A interface area.²⁻⁴ This type of architecture, dubbed bulk heterojunction usually allows for light absorption in the bulk donor domains that generate excitons, followed by exciton dissociation at the D-A interfaces. However, the process by which the excitons reach the D-A interfaces and dissociate to generate separate charge polarons in the D-A nano-domains is only now becoming the focus of attention.^{5,6}

It was originally postulated that, once the exciton in the bulk donor domain reaches the D-A interface, it undergoes an ultrafast electron transfer to the acceptor forming a hole-polaron (P⁺) in the donor and electron-polaron (P⁻) in the acceptor, which are free to participate in the subsequent charge transport process towards the device electrodes.⁷ However, the mutual P⁺-P⁻ Coulomb attraction should prevent a complete charge separation even if the offset energy of the donor and acceptor active levels is taken into account.⁸ On the contrary, the bound P⁺-P⁻ pair forms a charge transfer (CT) state at the D-A interface deep below the D and A optical gaps. However, in spite of ample spectroscopic evidence for the existence of such a CT state at the D-A interfaces,⁹⁻¹³ it has been argued that it lies too deep in the gap to have any effect on the charge photogeneration process in the blends.¹⁰

In this paper, we used the pump/probe transient photomodulation spectroscopy in an unprecedented broad spectral range to elucidate the early stages of the charge photogeneration

process in the prototype D-A blend, namely the donor polymer regio-regular (RR-) (3 hexyl thiophene) [P3HT; see Fig. 1(a) inset] and the fullerene acceptor molecule [6,6]-phenyl-C₆₁-butyric acid methyl ester [PCBM; Fig. 1(b) inset]. This blend shows separated D-A domains and consequently has high solar power conversion efficiency $\eta \sim 4\%$.¹³ Although there have been several studies on the photoexcitation dynamics of the P3HT/PCBM blend, many questions still remain unresolved regarding the role of the CT state on the charge generation processes.¹⁴⁻²⁵ We present compelling evidence that, after the photoexcited excitons in the polymer domains reach the D-A interfaces, the charge generation process proceeds via the formation of CT excitons at the interfaces. In RR-P3HT/PCBM with (1.2:1) weight ratio the photogenerated excitons in the polymer domain reach the D-A interfaces forming CT excitons within ~ 10 ps. In contrast, in regio-random (RRa)-P3HT/PCBM blend where the D and A domain sizes are much smaller, the CT excitons at the D-A interfaces are generated within ~ 200 fs. However, the subsequent exciton dissociation process in this blend is hampered by the large CT binding energy,¹¹ which explains the smaller η value ($< 0.1\%$) of solar cells based on this blend. Our findings support a two-step process for the charge photogeneration in organic D-A blends⁵ and emphasize the important role of the CT exciton binding energy in generating free charges in organic solar cells.

The P3HT polymers and PCBM fullerene were supplied by Plextronics Inc.¹³ The mixing ratio of the P3HT/PCBM blends was 1.2:1 by weight, which gives the optimal η value in solar cells.⁶ The films were spin cast onto CaF₂ or CsI that are transparent in the mid-infrared (IR) spectral range. The RR-P3HT/PCBM blend film was thermally annealed at 150 °C for 30 min to enhance the D-A domains size;⁶ whereas the RRa-P3HT/PCBM film was used as deposited.

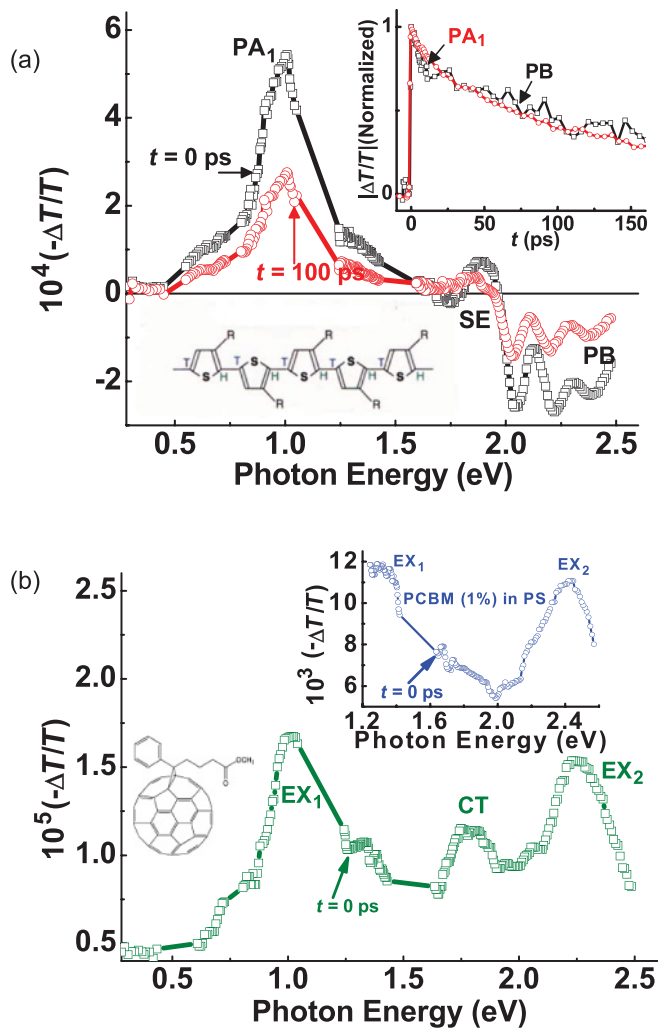


FIG. 1. (Color online) (a) The transient photomodulation spectrum of a pristine RR-P3HT film at $t = 0$ and 100 ps, respectively; the exciton bands PA₁, SE, and PB are indicated. The right inset shows the transient decay of PA₁ and PB bands up to $t = 160$ ps; the left inset shows the polymer backbone chain. (b) The transient photomodulation spectrum of a PCBM film at $t = 0$; the exciton PA bands EX₁ and EX₂, and CT exciton band are indicated. The right inset shows the $\Delta T/T(0)$ spectrum of isolated PCBM molecules in polystyrene (weight ratio of 1:100) that lacks the CT exciton band. The left inset shows the PCBM molecular structure.

For the polarized transient photomodulation spectroscopy, we used the femtosecond (fs) two-color pump/probe correlation technique with two different pulsed laser systems based on a Ti: Sapphire oscillator.²⁶ These are: a low-power (energy/pulse ~ 0.1 nJ) high-repetition rate (~ 80 MHz) pulsed laser system for the mid-IR spectral range, and a high-power (energy/pulse ~ 10 μ J) low-repetition rate (~ 1 kHz) pulsed laser system for the near-IR/visible spectral range. The pump excitation photon energy $\hbar\omega(\text{pump})$ was set at 3.1 eV for above-gap and 1.55 eV for below-gap excitation, respectively. The pulse energy flux on the film was adjusted so that the initial photoexcited exciton density $N(0) \approx 10^{16}/\text{cm}^3$ [$N(0) \approx 10^{17}/\text{cm}^3$] for the mid-IR (near-IR) laser system. For the probe in the mid-IR measurements, we used an optical parametric oscillator (OPAL, Spectra Physics) that generates

$\hbar\omega(\text{probe})$ ranging from 0.55 to 1.05 eV. In addition, we also used a difference-frequency crystal (AgGaS₂) and the signal and idler beams of the OPAL for generating $\hbar\omega(\text{probe})$ in the spectral interval 0.25 to 0.43 eV.¹¹ The pump beam was modulated at frequency $f = 40$ kHz, and the changes ΔT in the probe transmission T were measured using a phase-sensitive technique. For the transient near-IR/visible spectroscopy measurements, we used white light super-continuum as probe, spanning the spectral range from 1.15 to 2.5 eV; the pump modulation frequency here was synchronized with the laser repetition rate. The transient photomodulation signal $\Delta T/T$ is positive for photoinduced absorption (PA) and negative for photo-bleaching and stimulated emission. Here, $\Delta T(t)/T$ was measured using a computer-controlled translation stage up to 2 ns, with time resolution of ~ 150 fs set by the pump/probe cross-correlation. The $\Delta T(0)/T$ spectra from the two laser systems were normalized to each other at several wavelengths in the near-IR/visible spectral range.²⁶

Since some photoexcitations may live longer than the time interval between successive pulses, then a background PA may be formed. An advantage of the mid-IR laser system is that the background PA spectrum can be readily measured using the same pump/probe set up as for the ultrafast response. This was achieved by measuring the PA signal at $t < 0$ since the probe pulse in this situation arrives before the pump pulse and therefore is affected by the leftover photoexcitations in the film that survive in between successive pulses.²⁷ Recall that the background PA is modulated at a frequency of 40 kHz and thus is sensitive to long-lived photoexcitations in the film having lifetime longer than $\sim 1/f$ ($=25$ μ sec).

The bulk heterojunction OPV solar cell devices were composed of a transparent indium tin oxide (ITO) anode; a spin-cast polyethylenedioxythiophene/polystyrene sulphonate (PEDOT/PSS) hole transport layer; an active material layer spin-cast from a blend of a P3HT donor and a PCBM acceptor; and capped with an LiF/Al cathode. The ITO-coated glass substrates (Delta Technology, CB-50IN) were cleaned by ultrasonic treatment and oxygen plasma treatment. The PEDOT/PSS (Clevios, P VP AI 4083) layer was spin-cast at 5000 RPM for 20 s at ambient conditions and transferred to a nitrogen-filled glovebox ($\text{O}_2 < 1$ ppm) for annealing at 120 $^\circ\text{C}$ for 30 min. The organic blend comprised of P3HT (Plextronics, Plexcore OS 2100) and PCBM (purity $> 99.9\%$) were prepared at a weight ratio of 1.2:1 in 1,2-dichlorobenzene solution that was heated at 50 $^\circ\text{C}$ for 30 min and stirred overnight. The device active layer was spin-cast from the solution blend at 400 RPM for 6 min and annealed at 150 $^\circ\text{C}$ for 30 min; the device active area was 2×2.5 mm. The fabrication was completed by thermally evaporating a 1-nm-thick film of LiF layer followed by a 100-nm-thick film of Al. Finally, the device was encapsulated under a cover glass using UV-curable optical adhesive (Norland, NOA 61). The device I-V characteristics under illumination were measured using a Keithley 236 Source-Measure unit. The light intensity of the solar simulator composed of a xenon lamp and an AM1.5G filter was calibrated at 100 mW/cm² using a precalibrated silicon photovoltaic cell. The OPV device output current was measured using a phase sensitive lock-in technique.

In order to identify photogenerated polarons in the photomodulation spectrum, we also measured the doping-induced

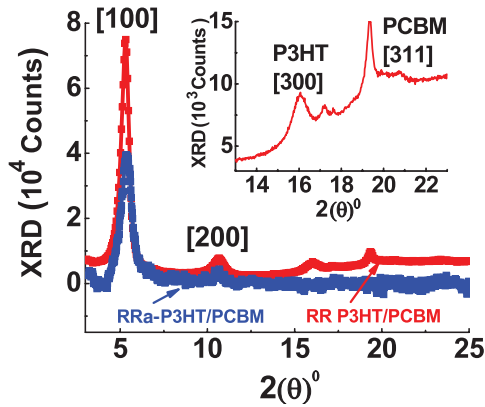


FIG. 2. (Color online) The XRD pattern from RRa-P3HT/PCBM (red) and RR-P3HT/PCBM (blue), where the P3HT bands [100], [200], and [300] and PCBM band [311] are assigned; the inset focuses on the PCBM band.

absorption spectrum in P3HT, where a thin polymer film was exposed to low-pressure iodine gas for ~ 10 s. The doping-induced absorption spectrum was then obtained by subtracting the optical density of the pristine polymer film from that of the doped film, as shown in the Fig. 3(a) inset. It is seen that the doping-induced absorption spectrum in RR-P3HT (and RRa-P3HT) is dominated by two absorption bands, namely P_1 and P_2 that peak at 0.1 and 1.8 eV, respectively,²⁸ which are due to delocalized hole-polarons on the polymer chains.

We first measured $\Delta T(t)/T$ spectra of pristine polymer and fullerene films (Fig. 1). The $\Delta T(0)/T$ spectrum of pristine RR-P3HT film [Fig 1(a)] is dominated by a single PA_1 band at 1 eV followed by photo-bleaching above 1.97 eV and a small stimulated emission band at 1.75 eV, which attests to the excellent quality of the RR-P3HT polymer used here.¹³ These three spectral features originate from photogenerated excitons since they decay together [Fig. 1(a) right inset] with an exponential time constant $\tau_0 = 70$ ps. No photogenerated polarons of which PA peaks at 0.1 and 1.8 eV [see Fig. 3(a) inset] are observed here. Figure 1(b) shows the $\Delta T(0)/T$ spectrum of pristine PCBM film. It is dominated by two PA bands, namely EX_1 and EX_2 at 1.0 and 2.25 eV, respectively, that are due to photogenerated excitons. A third PA band, CT at 1.75 eV, originates from charge-transfer excitons in the fullerene film since it does not exist in the photomodulation spectrum of isolated PCBM molecules in polystyrene [Fig. 1(b) right inset]. No photogenerated polarons of which PA peaks at 1.15 eV^{29,30} are discerned.

To better understand the transient PA spectra in the polymer/fullerene blends, we measured the x-ray diffraction (XRD) pattern from the RRa- and RR-P3HT/PCBM blend films (Fig. 2) using the $CuK\alpha$ x-ray line at $\lambda = 0.154$ nm. The XRD pattern of RR-P3HT/PCBM contains a prominent Bragg band at $2\theta_{[100]} = 5.3^\circ$ and its harmonics at $2\theta = 10.7^\circ$ and 16° , respectively, that originate from the P3HT nanocrystalline domains in the film;³¹ as well as a smaller Bragg band at $2\theta_{[311]} = 19.3^\circ$ that originates from the PCBM nanocrystalline domains in the blend.³² We therefore conclude that the annealed RR-P3HT/PCBM blend film contains separate donor and acceptor crystalline domains. We may estimate the average nanocrystalline domain size D from the full width at half

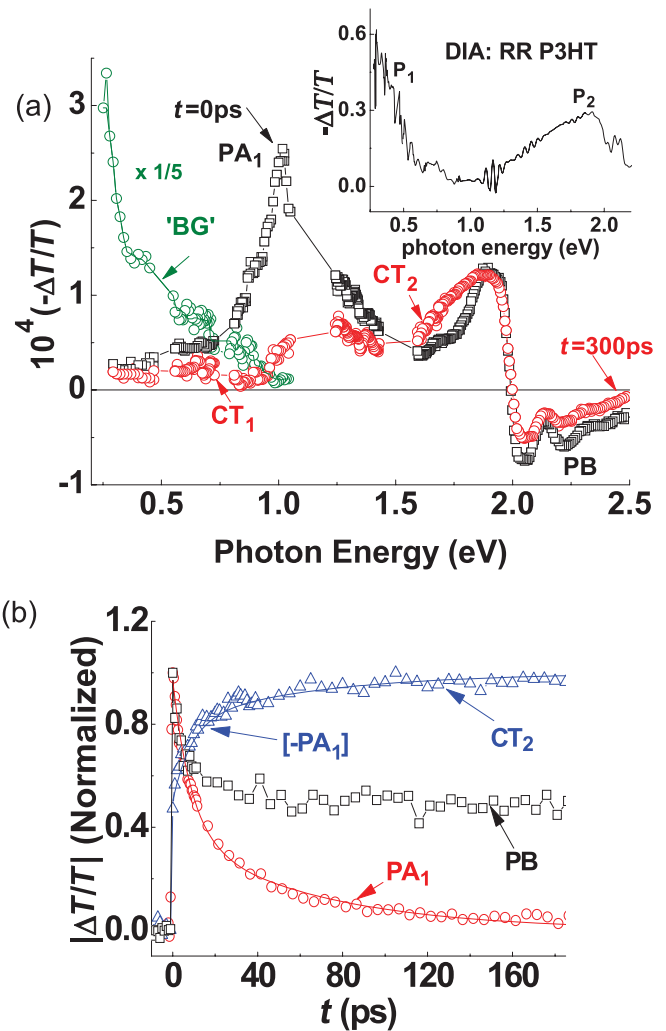


FIG. 3. (Color online) (a) The transient photomodulation spectrum of an RR-P3HT/PCBM blend film at $t = 0$ and 300 ps, respectively; the exciton band PA_1 and CT exciton bands CT_1 and CT_2 are indicated. The green circles and line represent the background (BG) PA spectrum measured at $t = -5$ ps. The inset shows the doping-induced absorption of a pristine RR-P3HT film, where the polaron bands P_1 and P_2 are assigned. (b) The transient decay of PA_1 , buildup dynamics of CT_2 , and the PB decay up to 180 ps. The line through the data points is a fit using the FRET mechanism (see text); the same function also fits the CT_2 buildup dynamics.

maximum $\Delta_{2\theta}$ of the respective Bragg bands using the Scherrer relation: $D = 0.9\lambda / \Delta_{2\theta} \cdot \cos \theta$; we obtain $D \approx 16$ nm (20 nm) for the polymer (PCBM) nano-domains. In contrast, the XRD pattern of the RRa-P3HT/PCBM blend does not show prominent P3HT band harmonics, and in addition the PCBM band is missing (Fig. 2). These indicate that the PCBM molecules do not form well-separated domains here; instead, they penetrate into the P3HT lamellae and consequently are much closer on average to the polymer chains.

Figure 3(a) shows the $\Delta T(t)/T$ spectra of the RR-P3HT/PCBM blend. The $\Delta T(0)/T$ spectrum is very similar to that of pristine RR-P3HT [Fig. 1(a)], indicating that excitons are initially photogenerated within the polymer domains. At $t > 0$, the excitons decay; however, no polarons are generated at the expense of the exciton decay up to 300 ps since there is

no PA buildup at low $h\omega$ (probe), where the polaron P_1 band dominates the absorption spectrum [as seen in the Fig. 3(a) inset]. We thus conclude that the photogenerated excitons in the polymer domains decay into a new state that is not separated free polarons. This new state must be related with the D-A interfaces in the films since the excitons do not form such a state in the pristine polymer, and we thus propose that is a CT exciton at the D-A interface. In contrast, the background PA spectrum in the mid-IR [Fig. 3(a)] is very similar to the P_1 band in the polaron doping-induced absorption spectrum [Fig. 3(a) inset], showing that charge polarons are indeed photogenerated in this RR-P3HT/PCBM film but at later time, in agreement with the high solar cells efficiency based on this blend.¹³ We thus conclude that the charge photogeneration process in the blend proceeds in two stages.^{5,16} The first stage is exciton trapping in CT states at the D-A interfaces followed by a much slower exciton dissociation into free polarons in the D and A domains at $t \gg 2$ ns (=the time limit of our translation stage).

The exciton decay dynamics in the blend are much faster than in the pristine polymer [see PA_1 decays in Figs. 3(a) and 1(a)]. The shorter lifetime in the blend is related to the exciton dynamics towards the D-A interfaces, and therefore we studied the PA_1 decay kinetics in more detail. Here, PA_1 decay cannot be fit with a single or a few exponential decay functions; nor can it be fit using a diffusion model $\sim (1 + t/\tau)^{-1}$. Alternatively, PA_1 decay can be fit using multiple power-law decays that originate from a Förster resonant energy transfer (FRET) into the CT exciton,³³ averaged over the exciton initial distance from the D-A interface (see the Appendix). This model yields the following time-dependent surviving exciton density $N(t)$ in the polymer nano-grains:

$$\frac{N(t)}{N(0)} = \exp\left(-\frac{t}{\tau_0}\right) \left[m_1 + m_2(C_1 t^{1/2} - C_2 t^{1/3} + C_3 t^{1/6}) \right], \quad (1)$$

where $\tau_0 = 70$ ps is the natural exciton lifetime in RR-P3HT that is obtained from the PA_1 dynamics of Fig. 1; m_1 and m_2 are fitting parameters; and the C constants are given by the relations: $C_1 = 0.2u^{-3}$, $C_2 = 0.66u^{-2}$ and $C_3 = 0.54/u$, where $u = D/2R_0$ is the parameter ratio of the grain size D to twice the FRET radius R_0 , which was measured before to be between 3 and 9 nm.³⁴ Using $R_0 = 6$ nm and $D = 16$ nm from the XRD studies, we obtain $u = 1.3$. Subsequently, the excellent fit to the PA_1 decay seen in Fig. 3(b) was obtained using $m_1 = 0.14$ and $m_2 = 7$.

In support of the CT intermediate role in the charge photogeneration process in the blend, Fig. 3(a) also shows that PA buildup indeed occurs in both mid-IR and near-IR³⁵ spectral ranges. In fact there are two PA bands, namely CT_1 in the mid-IR and CT_2 in the near-IR, that are generated at longer time at the expense of the exciton PA_1 decay. Figure 3(b) shows that the CT_2 buildup dynamics in the near-IR closely matches the exciton PA_1 decay since the same function of time fits both PA_1 decay and CT_2 buildup dynamics (measured at 1.75 eV probe). Figure 4(a) more clearly shows the two PA bands that are generated at the expense of the exciton PA_1 decay. To obtain the full photogenerated CT spectrum, we subtracted the photomodulation spectrum at $t = 30$ ps from that at $t = 0$

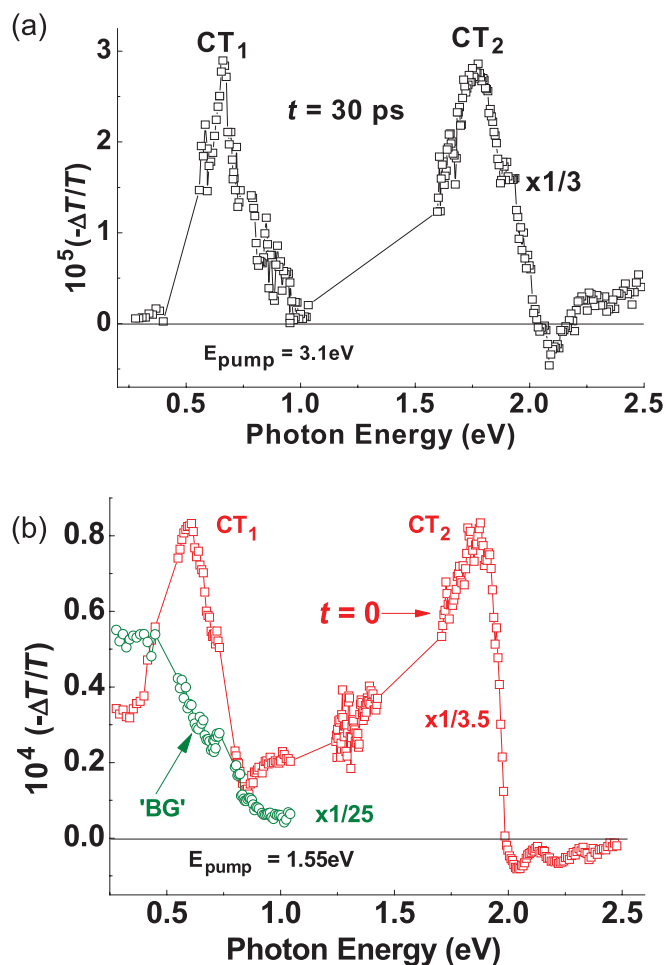


FIG. 4. (Color online) (a) The transient photomodulation spectrum of an RR-P3HT/PCBM blend film at $t = 30$ ps excited at 3.1 eV, normalized and subtracted from the spectrum at $t = 0$, that shows the two newly formed CT_1 and CT_2 bands. (b) Same as in (a) but at $t = 0$ and excited at 1.55 eV, which is below the gap of both polymer and fullerene constituents.

after normalizing the two PA bands at 1 and 2 eV for the CT_1 and CT_2 bands, respectively. It is seen that the CT spectrum contains two prominent PA bands that peak at 0.6 (CT_1) and 1.75 eV (CT_2), respectively, which are very different than the bands P_1 and P_2 of polarons [Fig. 3(a) inset]. Consequently, we propose that these two PA bands are due to optical transitions within the CT manifold at the D-A interfaces.^{5,8}

To support this assumption, we measured the transient photomodulation spectrum using $h\omega(\text{pump}) = 1.55$ eV, which is below the optical gap of the polymer and fullerene constituents. Such low $h\omega(\text{pump})$ can resonantly excite the CT state at the D-A interface since its energy was measured to be between 1.2 to 1.6 eV,¹³ without first photogeneration of excitons in the polymer domains. Figure 4(b) shows that, under these conditions, the two CT PA bands are instantaneously photogenerated, which is compelling evidence that they originate from the CT states at the interfaces. This supports our assignment for the CT bands in the transient photomodulation spectrum of this blend.

Interestingly, the background PA spectrum excited with below-gap pump excitation [Fig. 4(b)] is very similar to that

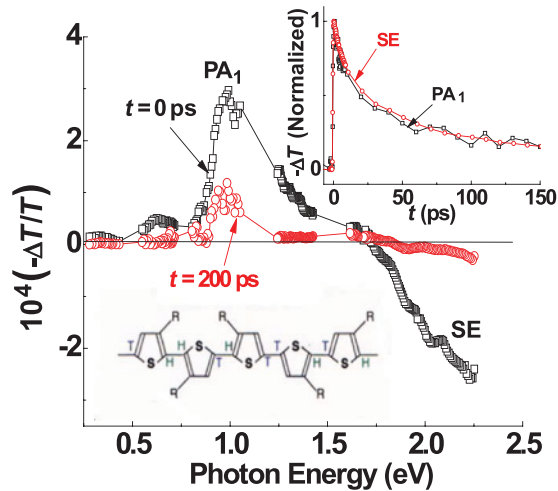


FIG. 5. (Color online) The transient photomodulation spectrum of a pristine RRa-P3HT film at $t = 0$ and 200 ps, respectively; the exciton bands PA₁ and SE are indicated. The right inset shows the transient decay of PA₁ and SE bands up to $t = 150$ ps; the left inset shows the polymer backbone chain.

generated using above-gap pump excitation [Fig. 3(a)], which we identified as due to long-lived charge polarons.¹³ This shows that there exists a mechanism where thermalized CT excitons at the D-A interfaces are able to separate into free polarons in the donor and acceptor domains, regardless of the initial $h\omega(\text{pump})$.⁵ This finding is very important since it can refute the notion that the CT state in the blend lies too deep in the gap to have any influence over the charge photogeneration process. Apparently, the exciton kinetic energy when reaching the CT state plays a minor role in the charge photogeneration process; this may explain the flat spectral response of the photocurrent action spectrum in organic solar cells.¹³

For comparison, we also study the charge photogeneration mechanism in RRa-P3HT/PCBM blend where the fullerene molecules are closer to the polymer chains on average. Figure 5(a) shows $\Delta T(t)/T$ spectra of pristine RRa-P3HT. It also contains a single PA₁ exciton band at ~ 1 eV followed by stimulated emission above ~ 1.75 eV that shares the same dynamics [Fig. 5(a) inset]. However, the $\Delta T(0)/T$ spectrum in the RRa-P3HT/PCBM blend [Fig. 6(a)] is very different from that in the RR-P3HT/PCBM blend [Fig. 3(a)]. The former spectrum shows the same two CT PA bands (namely CT₁ and CT₂ discussed above) that are generated within ~ 500 fs [Fig. 6(b)] in concert with the ultrafast decay of the exciton PA₁ band. The fast exciton decay here is consistent with the proximity of the PCBM molecules to the P3HT polymer chains in the RRa-P3HT/PCBM blend. Interestingly, the background PA spectrum here does not show long-lived polaron photogeneration; in fact, the background PA spectrum is the same as the transient PA spectrum. This shows that the photogenerated CT excitons in this blend cannot easily dissociate into free polarons, in agreement with the poor solar cell efficiency ($< 0.1\%$) based on this blend (Fig. 7). It also shows that the CT exciton dissociation is related to the D-A domain size. The larger the D-A interface area, the smaller the CT exciton binding energy, and consequently the

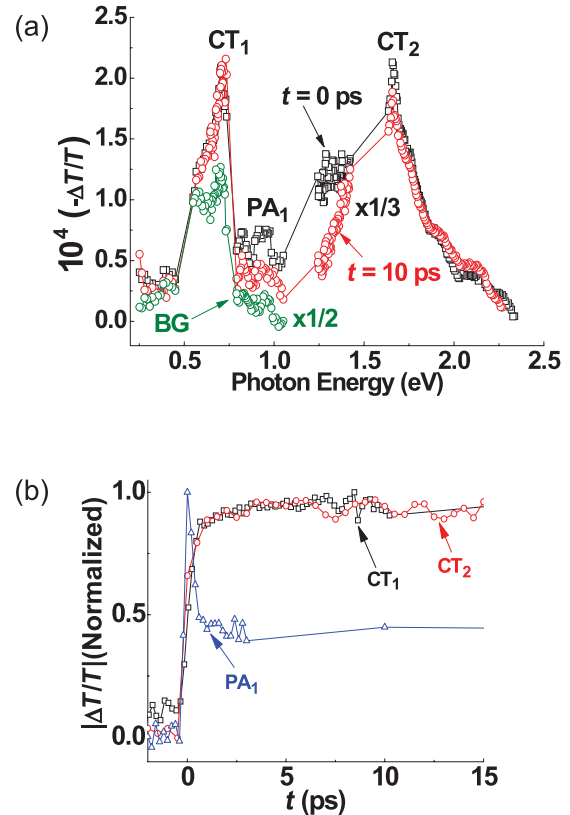


FIG. 6. (Color online) (a) The transient photomodulation spectrum of an RRa-P3HT/PCBM blend at $t = 0$ (black squares) and 10 ps (red circles), respectively, excited at 3.1 eV; the PA bands PA₁, CT₁, and CT₂ are assigned. The background PA is also shown (green circles) up to 1 eV. (b) The transient decay of PA₁ and buildup dynamics of CT₁ and CT₂ up to 15 ps.

more efficient the CT exciton dissociation into separate charge polarons in the D and A domains.³⁶

This conclusion is further supported by the I-V characteristics under solarlike illumination of photovoltaic devices based on RR-P3HT/PCBM and RRa-P3HT/PCBM blends

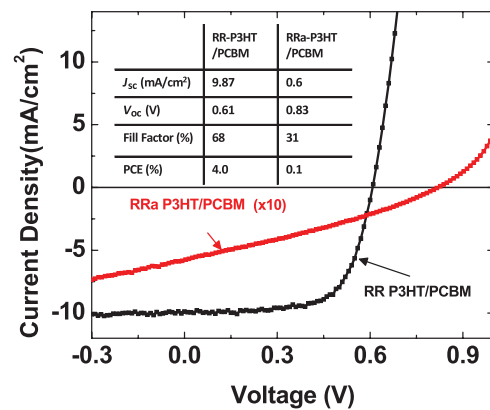


FIG. 7. (Color online) The I-V characteristic of two solar cells based on the PCBM blend with RR-P3HT (black) and RRa-P3HT (red) donor polymers under solarlike illumination of AM 1.5. The inserted table gives the device photovoltaic characteristic parameters such as short-circuit current density J_{sc} , open-circuit voltage V_{oc} , fill-factor FF, and the power conversion efficiency PCE in %.

using an AM1.5 filter as shown in Fig. 7. It is seen that the power conversion efficiency and short circuit current of the RR-P3HT/PCBM blend are more than an order of magnitude higher than that of the RRa-P3HT/PCBM blend.

In summary, using the ps transient pump/probe photo-modulation technique in P3HT/PCBM blends with typical D-A bulk heterojunction morphology, we demonstrated that the charge photogeneration mechanism in organic solar cells occurs in two steps. First, the photogenerated excitons in the polymer domains reach the D-A interfaces within a few ps time depending on the domain size, where they form CT excitons. This process is followed by CT exciton dissociation into free charged polarons in the D and A domains in the ns- μ sec timescale, which remains to be observed. The CT exciton dissociation depends on the CT binding energy, which is significantly lower for larger D-A interface area. Our results emphasize the importance of the D-A domain size in organic solar cells based on bulk heterojunction morphology.

ACKNOWLEDGMENTS

We acknowledge the assistance of Y. Zhang in measuring the XRD pattern. This work was supported in part by the DOE Grant No. DE-FG02-04ER46109 at the University of Utah.

APPENDIX: DERIVATION OF FÖRSTER ENERGY TRANSFER DYNAMICS FOR EXCITONS IN THE POLYMER GRAINS

We assume that the polymer grains are spherical, having radius R [Fig. 8(a)]. Also, we hypothesize that the Förster energy transfer (FRET) kinetics from a point r inside the polymer grain to its surface is exponential in nature.³³ Therefore, the surviving exciton density inside the polymer

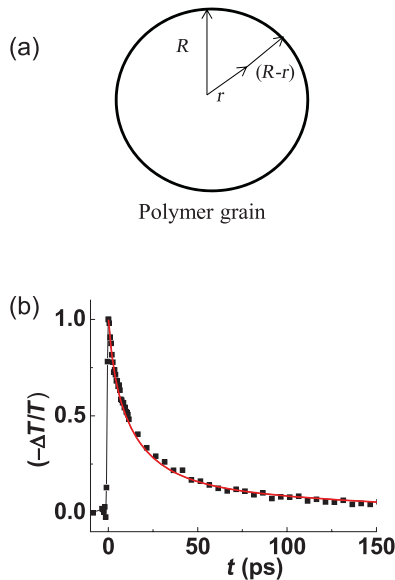


FIG. 8. (Color online) (a) Schematic diagram of the polymer grain of radius R , where r is the exciton distance from the center. (b) The decay of the PA₁ band in the RR-P3HT/PCBM blend, measured at 1 eV probe photon energy. The decay is fit using Eq. (A6) with the parameters given in the Appendix.

grain at point r can be written as follows:

$$n(t) = n(0) \exp[-v(r)t], \quad (\text{A1})$$

where $v(r) = v_o \frac{R_o^6}{(R-r)^6}$ and R_o is the FRET radius. In order to calculate the total surviving exciton density $N(t)$ inside the polymer grain, we integrate over the distance r normalized by the sphere volume:

$$N(t) = N(0) \frac{\int_0^{R_{\min}} \exp(-v(r)t) 4\pi r^2 dr}{4\pi R^3/3}. \quad (\text{A2})$$

Here, R_{\min} is the distance from the center where $v(r)$ reaches its maximum rate v_{\max} and thus does not change with r for $r > R_{\min}$. Equation (A2) can also be written in terms of the exciton lifetime τ :

$$N(t) = N(0) \frac{\int_{\tau_{\min}}^{\tau_{\max}} \exp\left(-\frac{t}{\tau}\right) g(\tau) d\tau}{4\pi R^3/3}, \quad (\text{A3})$$

where $\frac{1}{\tau} = \frac{1}{\tau_o} \frac{R_o^6}{(R-r)^6}$ and τ_o is the exciton natural decay lifetime in the bulk polymer. Writing for simplicity $R = \mu R_o$, where μ is a constant ($\mu < 1$), we can substitute the distance r and lifetime τ using μ : $r = R_o[\mu - (\frac{\tau}{\tau_o})^{1/6}]$ and $dr = -\frac{R_o}{6\tau_o^{1/6}} \tau^{-5/6} d\tau$. Substituting these relations in Eq. (A2), we obtain the following equation for $N(t)$:

$$\frac{N(t)}{N(0)} = \frac{\exp\left(-\frac{t}{\tau_o}\right)}{2\mu^3 \tau_o^{1/6}} \int_{\tau_{\min}}^{\tau_{\max}} \frac{\exp\left(-\frac{t}{\tau}\right)}{\tau^{5/6}} \times \left[\mu^2 + \left(\frac{\tau}{\tau_o}\right)^{1/3} - 2\mu \left(\frac{\tau}{\tau_o}\right)^{1/6} \right] d\tau. \quad (\text{A4})$$

Replacing $X = \frac{t}{\tau}$ and assuming $X_{\min} = 0.1$ and $X_{\max} = \infty$, we then obtain:

$$\frac{N(t)}{N(0)} = \exp\left(-\frac{t}{\tau_o}\right) \left\{ m_1 + m_2 \left[\left(\frac{0.542}{\mu}\right) t^{1/6} - \left(\frac{0.66}{\mu^2}\right) t^{1/3} + \left(\frac{0.203}{\mu^3}\right) t^{1/2} \right] \right\}. \quad (\text{A5})$$

The above expression is derived for a single grain size R . For simplicity, we assume that most polymer grains are of size R_{avg} , where $R_{\text{avg}} = \mu_{\text{avg}} R_o$. Including μ_{avg} into Eq. (A5), we finally get Eq. (A6) [or Eq. (1) in the text] for the decay of excitons in the polymer blend:

$$\frac{N(t)}{N(0)} = \exp\left(-\frac{t}{\tau_o}\right) \left\{ m_1 + m_2 \left[\left(\frac{0.542}{\mu_{\text{avg}}}\right) t^{1/6} - \left(\frac{0.66}{\mu_{\text{avg}}^2}\right) t^{1/3} + \left(\frac{0.203}{\mu_{\text{avg}}^3}\right) t^{1/2} \right] \right\}. \quad (\text{A6})$$

We found that the best fit to PA₁ decay was obtained using $m_2 = 7$ and $\mu_{\text{avg}} = 1.3$, as seen in Fig. 8(b). Using this μ_{avg} and $R_o = 6$ nm, the average grain diameter D of the polymer in the RR-P3HT/PCBM [1.2:1] blend ~ 16 nm, which is in good agreement with our XRD measurements described in Fig. 2.

*Present address: School of Electrical and Computer Engineering, Georgia Institute of Technology, Atlanta, GA.

†These two authors contributed equally.

‡Corresponding author: valy_vardeny@yahoo.com

¹M. R. Wasielewski, *Chem. Rev.* **92**, 435 (1992).

²X. N. Yang, J. Loos, S. C. Veenstra, W. J. H. Verhees, M. M. Wienk, J. M. Kroon, M. A. J. Michels, and R. A. J. Janssen, *Nano Lett.* **5**, 579 (2005).

³M. Campoy-Quiles, T. Ferenczi, T. Agostinelli, P. G. Etchegoin, Y. Kim, T. D. Anthopoulos, P. N. Stavrinou, D. D. C. Bradley, and J. Nelson, *Nat. Mater.* **7**, 158 (2008).

⁴R. A. Marsh, J. M. Hodgkiss, S. A. Seifried, and R. H. Friend, *Nano Lett.* **10**, 923 (2010).

⁵A. A. Bakulin, A. Rao, V. G. Pavelyev, P. H. M. van Loosdrecht, M. S. Pshenichnikov, D. Niedzialek, J. Cornil, D. Beljonne, and R. H. Friend, *Science* **335**, 1340 (2012).

⁶G. Li, R. Zhu, and Y. Yang, *Nature Photon.* **6**, 153 (2012).

⁷N. S. Sariciftci, L. Smilowitz, A. J. Heeger, and F. Wudl, *Science* **258**, 1474 (1992).

⁸X. Y. Zhu, Q. Yang, and M. Muntwiler, *Acc. Chem. Res.* **42**, 1779 (2009).

⁹J. J. Benson-Smith, L. Goris, K. Vandewal, K. Haenen, J. V. Manca, D. Vanderzande, D. D. C. Bradley, and J. Nelson, *Adv. Funct. Mater.* **17**, 451 (2007).

¹⁰T. Drori, C. X. Sheng, A. Ndohe, S. Singh, J. Holt, and Z. V. Vardeny, *Phys. Rev. Lett.* **101**, 037401 (2008).

¹¹M. Hallerman, S. Haneder, and E. Da Como, *Appl. Phys. Lett.* **93**, 053307 (2008).

¹²A. A. Bakulin, S. A. Zapunidy, M. S. Pshenichnikov, P. H. M. van Loosdrecht, and D. Y. Paraschuk, *Phys. Chem. Chem. Phys.* **11**, 7324 (2009).

¹³T. Drori, J. Holt, and Z. V. Vardeny, *Phys. Rev. B* **82**, 075207 (2010).

¹⁴I. A. Howard, R. Mauer, M. Meister, and F. Laquai, *J. Am. Chem. Soc.* **132**, 14866 (2010).

¹⁵H. Aarnio, P. Sehati, S. Braun, M. Nyman, M. P. D. Jong, M. Fahlman, and R. Österbacka, *Adv. Ener. Mat.* **1**, 792 (2011).

¹⁶J. Lee, K. Vandewal, S. R. Yost, M. E. Bhalke, L. Goris, M. A. Baldo, J. V. Manca, and T. V. Voorhis, *J. Am. Chem. Soc.* **132**, 11878 (2010).

¹⁷S. Cook, R. Katoh, and A. Furube, *J. Phys. Chem. C* **113**, 2547 (2009).

¹⁸G. Grancini, D. Polli, D. Fazzi, J. Gonzalez, G. Cerullo, and G. Lanzani, *J. Phys. Chem. Lett.* **2**, 1099 (2011).

¹⁹I. A. Howard and F. Laquai, *Macromol. Chem. Phys.* **211**, 2063 (2010).

²⁰D. Veldman, S. C. J. Meskers, and R. A. J. Janssen, *Adv. Funct. Mater.* **19**, 1939 (2009).

²¹K. Vandewal, K. Tvingstedt, A. Gadisa, O. Inganäs, and J. V. Manca, *Nature Mater.* **8**, 904 (2009).

²²P. E. Keivanidis, T. M. Clarke, S. Lilliu, T. Agostinelli, J. E. Macdonald, J. R. Durrant, D. D. C. Bradley, and J. Nelson, *J. Phys. Chem. Lett.* **1**, 734 (2010).

²³E. W. Snedden, A. P. Monkman, and F. B. Dias, *J. Phys. Chem. C* **116**, 86 (2012).

²⁴P. Parkinson, J. L. Hughes, M. B. Johnston, and L. M. Herz, *Phys. Rev. B* **78**, 115321 (2008).

²⁵J. L. Bredas, J. E. Norton, J. Cornil, and V. Coropceanu, *Acc. Chem. Res.* **42**, 1691 (2009).

²⁶C. X. Sheng, M. Tong, S. Singh, and Z. V. Vardeny, *Phys. Rev. B* **75**, 085206 (2007).

²⁷J. Holt, Ph.D. thesis, University of Utah, 2009.

²⁸X. M. Jiang, R. Österbacka, O. Korovyanko, C. P. An, B. Horowitz, R. A. J. Janssen, and Z. V. Vardeny, *Adv. Funct. Mater.* **12**, 587 (2002).

²⁹S. Yamamoto, J. Guo, H. Ohkita, and S. Ito, *Adv. Funct. Mater.* **18**, 2555 (2008).

³⁰J. Guo, H. Ohkita, H. Benten, and S. Ito, *JACS* **132**, 6154 (2010).

³¹H. Sirringhaus, P. J. Brown, R. H. Friend, M. M. Nielsen, K. Bechgaard, B. M. W. Langeveld-Voss, A. J. H. Spiering, R. A. J. Janssen, E. W. Meijer, P. Herwig, and D. M. de Leeuw, *Nature* **401**, 685 (1999).

³²P. H. Heiney, J. E. Fischer, A. R. McGhie, W. J. Romanow, A. M. Denenstien, J. P. McCauley, A. B. Smith, and D. E. Cox, *Phys. Rev. Lett.* **66**, 2911 (1991).

³³T. Förster, *Discuss. Faraday Soc.* **27**, 7 (1959).

³⁴D. C. Coffey, A. J. Ferguson, N. Kopidakis, and G. Rumbles, *ACS Nano* **4**, 5437 (2010).

³⁵I. W. Hwang, D. Moses, and A. J. Heeger, *J. Phys. Chem. C* **112**, 4350 (2008).

³⁶V. I. Arkhipov, P. Heremans, and H. Bässler, *Appl. Phys. Lett.* **82**, 4605 (2003).